Characterization of a planar 8 mm wide RF atmospheric pressure (bio-) plasma source by spectroscopy techniques.

Anton Yu Nikiforov[1, a)], Eusebiu-Rosini Ionita[2], Gheorghe Dinescu[2], and Christophe Leys[1]

Department of Applied Physics, Ghent University, Sint-Pietersnieuwstraat 41 B4, 9000 Gent, Belgium

National Institute of Laser, Plasma and Radiation, Magurele-Bucharest, MG-36, Ilfov RO 077125, Romania

Corresponding author's e-mail: anton.nikiforov@ugent.be

Classification numbers: ***PACS:*** **52.70.Kz, 52.80.Tn**

Atmospheric pressure planar RF 13.56 MHz discharge in Ar gas generated in long gap is investigated. The discharge operation with and without dielectric barrier on the electrodes is studied as a function of the applied power and gas flow. The source afterglow is characterized and analyzed for possible large scale biomedical applications where low gas temperature is required. The discharge is studied by relative and absolute emission spectroscopy. The gas temperature as low as 330±50 K is determined from rotational-vibrational band of OH emission. The absolute value of the discharge continuum irradiation is used to determine the electron density and the electron temperature. The electron-atom and electron-ion contributions to the Bremsstrahlung radiation are calculated and compared with measured spectra. The electron density of $1.9\pm1\times10^{20}$ m^{-3} and electron temperature of 1.75±0.25 eV are measured in the discharge without dielectric barrier. It is found that presence of the dielectric has negligible effect on electron temperature whereas electron number density is almost 6 times lower in the discharge with dielectric barrier.

1. Introduction

In the last decades, atmospheric pressure plasma jets (APPJs) have been extensively investigated in various new and fast growing interdisciplinary research and application fields [1,2]. The cold plasma jet will not damage the material to be processed with plasma, thus becomes suitable for processing: biologic matter, liquids, surfaces of living organisms, polymers, wood, textiles, etc. These processing at atmospheric pressure are performed without being limited by a vacuum chamber and without costs of vacuum generation. Unfortunately, the radial dimensions of the reported APPJs are mainly very small, which is a major drawback and limitation for some large-scale applications. To overcome the shortcoming, some exploratory researches have been done in the last years and variety of up-scale strategies for APPJs has been proposed. A ten-channel atmospheric pressure glow discharge jet has been purposed by Cao *et al* [3]. Nie reported a two-dimensional array of 7 jets with honeycomb configurations [4]. Moreover, he suggested that this configuration of array had no fundamental limitation to scale up and a 37-channel honeycomb-shaped array was presented to illustrate the scalability. The disadvantages of the use of plasma jet arrays are complex interaction between individual jets and extreme amount of the used expensive gases like Ar and even He, as has been observed by many researchers [5-8]. Another way to produce large area plasma source is an enlargement of the electrodes surface. A DC cold plasma brush (nozzle 10 mm × 1 mm) consisting of two cylindrical metallic electrodes with a perpendicular flowing Ar was reported by Duan *et al* [9,10]. Further enhancement on the DC brush was reported, such as the combination with a DBD reactor as a preionization source, the array of two DC brush with a transverse magnetic field [11-13]. Plasma brush driven by sub-microsecond voltage pulses was proposed by Lu *et al* [14]. M. Kong *et al.* [15] investigated possibility to generate RF plasma with 20 mm wide electrodes covered by dielectric. In [16] a large gap radio frequency (RF) discharge with one of the electrodes covered by dielectric (RF-DBD) has been generated in γ mode at atmospheric pressure in Ar as well as in N_2.

Nowaday constructed RF sources tested for use in large scale applications [17] can be classified mainly into two categories, considering the configuration of electrodes: one type is Dielectric Barrier Discharge (DBD), uses a dielectric barrier at one or at both electrodes [18,19] and the second type, Discharge with Bare Electrodes (DBE), having both electrodes in contact with the plasma [20,21]. For these two types of plasma sources there is no comparative study of the plasma parameters and effect of dielectric barrier on the discharge performance. For this reason we developed two jet plasma sources with different electrode configurations, one with DBD configuration and another one with DBE configuration. Unfortunately, the current knowledge of such discharges physics is very limited and very little is known about the discharge physics. This work is dealing with study of planar discharge with 8 mm wide outlet nozzle which is used to produce long and wide afterglow for biomedical applications. The sources studied here are identical apart from the use of dielectric barrier. The main parameters of the plasma including electron density n_e, electron temperature T_e, and gas temperature T_g are determined by different spectroscopy techniques as a function of operation parameters of the source, namely presence of the dielectric barrier, input power and gas flow rate. Special attention is paid to study of the plasma source continuum radiation which is used here to evaluate the n_e and T_e of the plasma through the simulation of the Bremsstrahlung radiation.

2. Experimental set-up and methods.

In current work two configurations of the planar RF discharge sources are studied. Both sources have the same discharge volume and architecture, working in similar conditions (RF power, gas type and flow rate) and so provide the opportunity to make a comparative study of the two types of discharges. Such a study could offer criteria for an optimization of the discharge operation and allocation of each source type in one application or another. Figure 1 presents a schematic view of the jet plasma sources in DBD and DBE configuration.

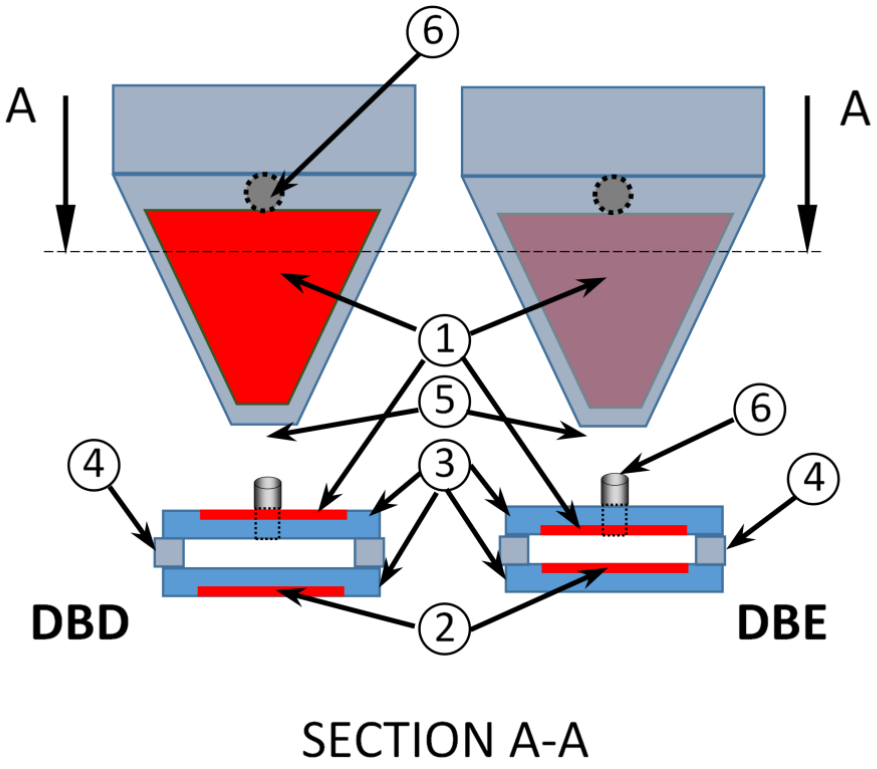

FIG. 1. Schematic view of DBD and DBE jet plasma sources. (1) RF electrode, (2)-GND electrode, (3)- Ceramic plates (dielectric), (4)-ceramic spacer, (5)-nozzle, (6)-gas intake hole.

The source is made of two trapezoidal ceramic plates (0.6 mm thick), spaced by ceramic holder (spacer) with 1 mm thickness. The spacers close the discharge space all around the electrode edges except in the front, at the small base of the trapezium, this represents the nozzle. The gas is introduced between ceramic plates through the intake hole, drilled in one ceramic plate. The interelectrodes gap is fixed at 1 mm through all the experiments. A compact aluminum house is used to hold the discharge configuration. Argon gas with flow rate in the range of 0.5-10 SLM is used as the working gas. There are two sheet metallic electrodes (RF and GND) placed in an exterior over the ceramic plates at DBD source and in an interior at DBE source, see Figure 1 (1) and (2). The electrodes are connected to a radio frequency generator (Advanced Energy Cesar 133RF) through a matching box. The applied

input power is varied in between 6 and 18 W with less than 5% of the reflected power in all the experiments. It has to be noted here that initiation of the breakdown requires much higher input power of up to 100 W. For safe control of the discharge initiation LabView software was developed in order to operate the RF generator through an acquisition board connected to the generator user analog port. This high power has been applied in 3 consequent pulses on 100 ms each and power has been reduced to desired low value right after the breakdown. At low power the discharge is ignited in diffuse mode where glow-like discharge fills the entire discharge space. Meanwhile, a brush-shape homogenous plasma afterglow is formed in the ambient air. Figure 2 shows the arrangement which was used in the work for basic characterization of the plasma source.

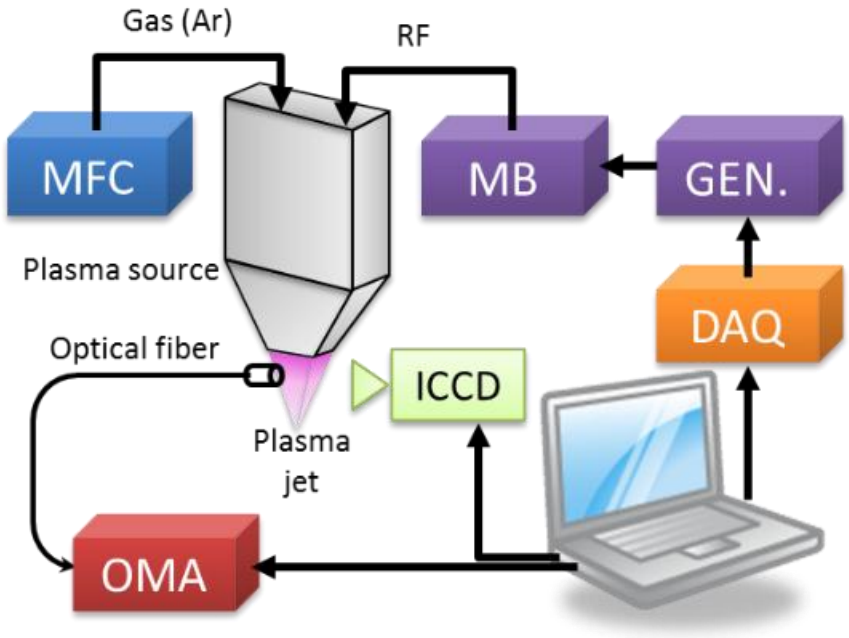

FIG. 2. The experimental set-up arrangement. Optical multichannel analyzer (OMA), Matching Box (MB), RF Generator (GEN.), Multifunction Data Acquisition (DAQ), Intensified Charge-Coupled Device (ICCD) and Mass Flow Controller (MFC).

The time integrated images of the discharge are recorded with the use of a Hamamatsu ICCD camera (C8484). The exposure time of the ICCD camera is adjusted in between the experiments for the highest contract of the images. The fast imaging is carried out with narrow band filters in order to detect OH radicals emission (309 nm), N_2^* emission (350-400 nm) and emission of Ar I line (753 nm). The optical emission spectrum is collected by two different spectrometers through the fiber optics. For a survey emission spectrum (250 – 850 nm), a S2000 Ocean Optics with a moderate resolution of 0.8 nm full width at half maxima (FWHM) is used. In order to obtain the gas temperature the high resolution spectrum of OH (A-X) bands is measured by an Avantes 3648 spectrometer with a resolution of 0.05 nm FWHM. The optical system is absolutely calibrated with an Oriel model 63355 tungsten-D_2 lamp and correspondingly the plasma irradiance in $Wm^{-2}nm^{-1}$ is measured. The experimental arrangement for

absolute OES measurement is schematically shown in figure 3. The plasma device is put 15 cm away from the detector in order to obtain the light projection of 1×1 cm^2 on the detector surface. An absorbing baffle with an aperture (0.8 × 0.8 cm^2) is placed between the jet source and the plane plate, and used to project the emission light from the discharge through the square aperture on the plate. All the three parts are centered precisely on the same optical axis with the help of a He-Ne laser beam. All the parts of the experimental arrangement mentioned above are fixed and identical for the calibration lamp and the plasma source. In this way, the spectral irradiance $I_{P,\lambda}(\lambda)$ from the plasma device can be represented as:

$$I_{P,\lambda}(\lambda) = \frac{h_{P,\lambda}(\lambda)}{h_{L,\lambda}(\lambda)} I_{L,\lambda}(\lambda)$$

where $I_{L,\lambda}(\lambda)$ ($Wm^{-2}nm^{-1}$) is the spectra irradiance of the calibration lamp, $h_{P,\lambda}(\lambda)$ and $h_{L,\lambda}(\lambda)$ are distance corrected relative emission intensities from the plasma and the lamp measured by the same OES system. All the measured values are time integrated and corrected for the background light.

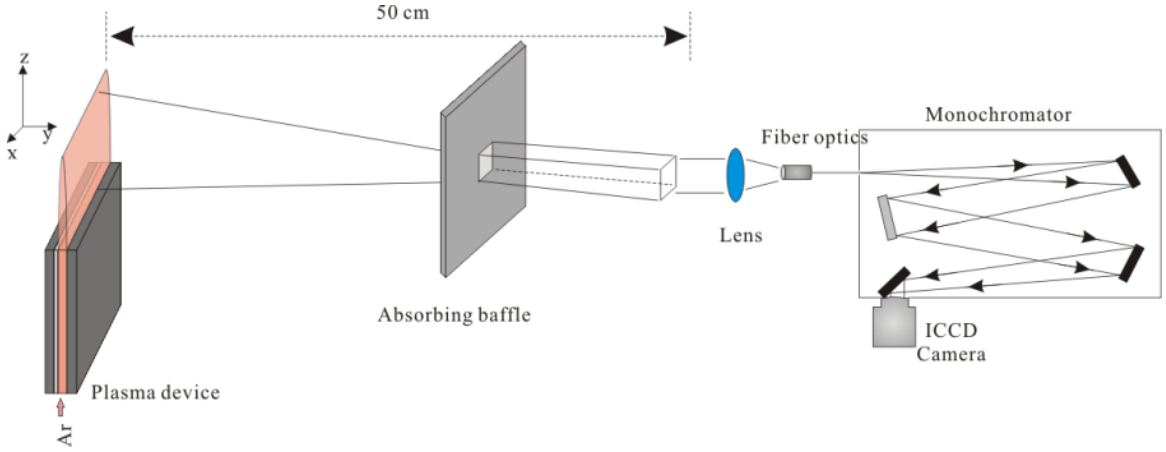

FIG. 3. Schematic diagram of the experimental setup for absolute OES measurements.

3. Results and discussion.

The application of RF high-voltage to the discharge gap leads to ignition of strongly filamentary γ mode discharge. The discharge can be sustained in a diffuse mode filling the entire discharge space by decrease of the input power. In diffuse α mode, a brush-shape homogenous plasma afterglow is generated along the slit in the ambient air with the total length of about 8 mm.

3.1. Emission spectrum of the discharge

To identify the various reactive species produced in the plasma afterglow, optical emission spectroscopy has been used. Figure 4 shows a typical emission spectrum of the plasma afterglow. The plasma spectrum is

dominated by the emission bands from $OH(A^2\Sigma^+ \rightarrow X^2\Pi)$, $N_2(C^3\Pi_u \rightarrow B^3\Pi_g)$, Ar I$(4p \rightarrow 4s)$, O I$(5p \rightarrow 5s)$, and strong continuum radiation in the range of 300-750 nm attributed to Bremsstrahlung radiation [23,24]. The presence of molecular bands of OH radicals and N_2 excited states allows estimating the gas temperature of the afterglow. As known [22], the energy transfer in between Ar metastables and N_2 leading to excitation of state $N_2(C)$ at high rotational levels makes difficult interpretation of the N_2 bands emission and so OH band has been used in the present work for the gas temperature calculation. The rotational temperature of the plasma was obtained through the analysis of $OH(A^2\Sigma^+ \rightarrow X^2\Pi)$ spectrum. In current study LIFBASE software has been used to simulate the spectrum but full explanation of the procedure is omitted here because it is well known method, well described in many other works [1,3,22]. The inset in Figure 4 shows the best-fitting synthetic spectrum to the experimental spectrum of the $OH(A^2\Sigma^+ \rightarrow X^2\Pi, \Delta v = 0)$ band transition from 306 nm to 312 nm, with rotational temperature of 330±50 K. The found value of T_g agrees well with the measurements by IR thermometer giving temperature of 340 K and clearly indicates low working temperature of the plasma source which is important parameter for possible biomedical application.

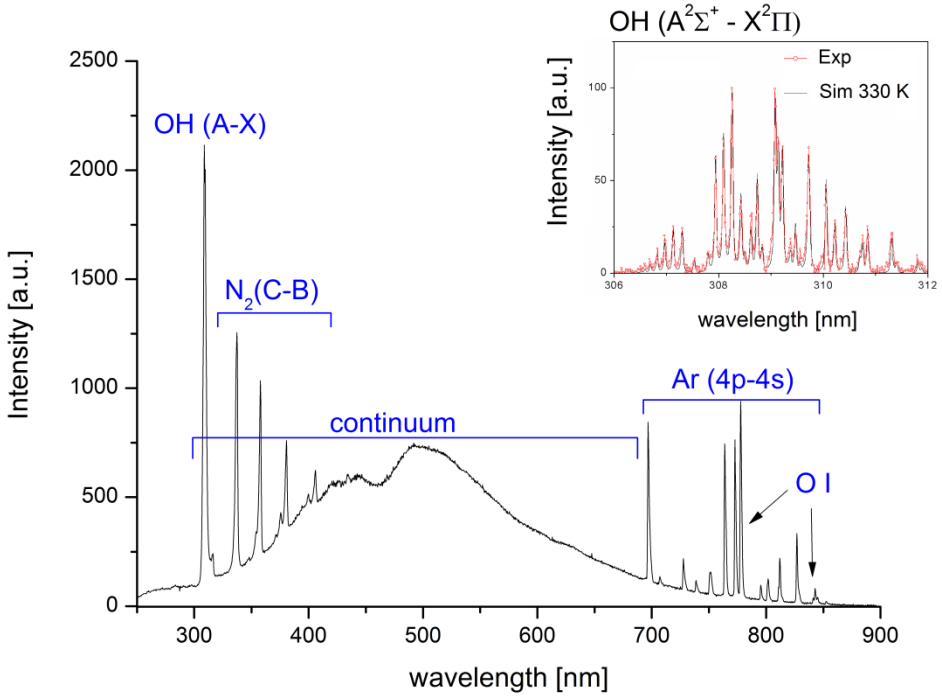

FIG. 4. Typical overview of the spectra of the discharge with dielectric barrier at 18 W and 10 slm Ar flow. The inset is an example of the best fit of the rotational structure of OH band by the simulation with T_{rot}=330 K. No spectrometer sensitivity correction has been applied to the spectra.

In Figures 5 and 6 optical emission intensities are plotted for specific lines, namely OH at 308.9 nm, N_2 second positive system at 337.1 nm, Ar I at 696.5 nm, and O I at 777.53 nm, as function of RF forward power and flow rate.

3D representation of the results has been performed through the use gridding method with extrapolation by Thin Plate Spline method implemented in Origin 8.0.

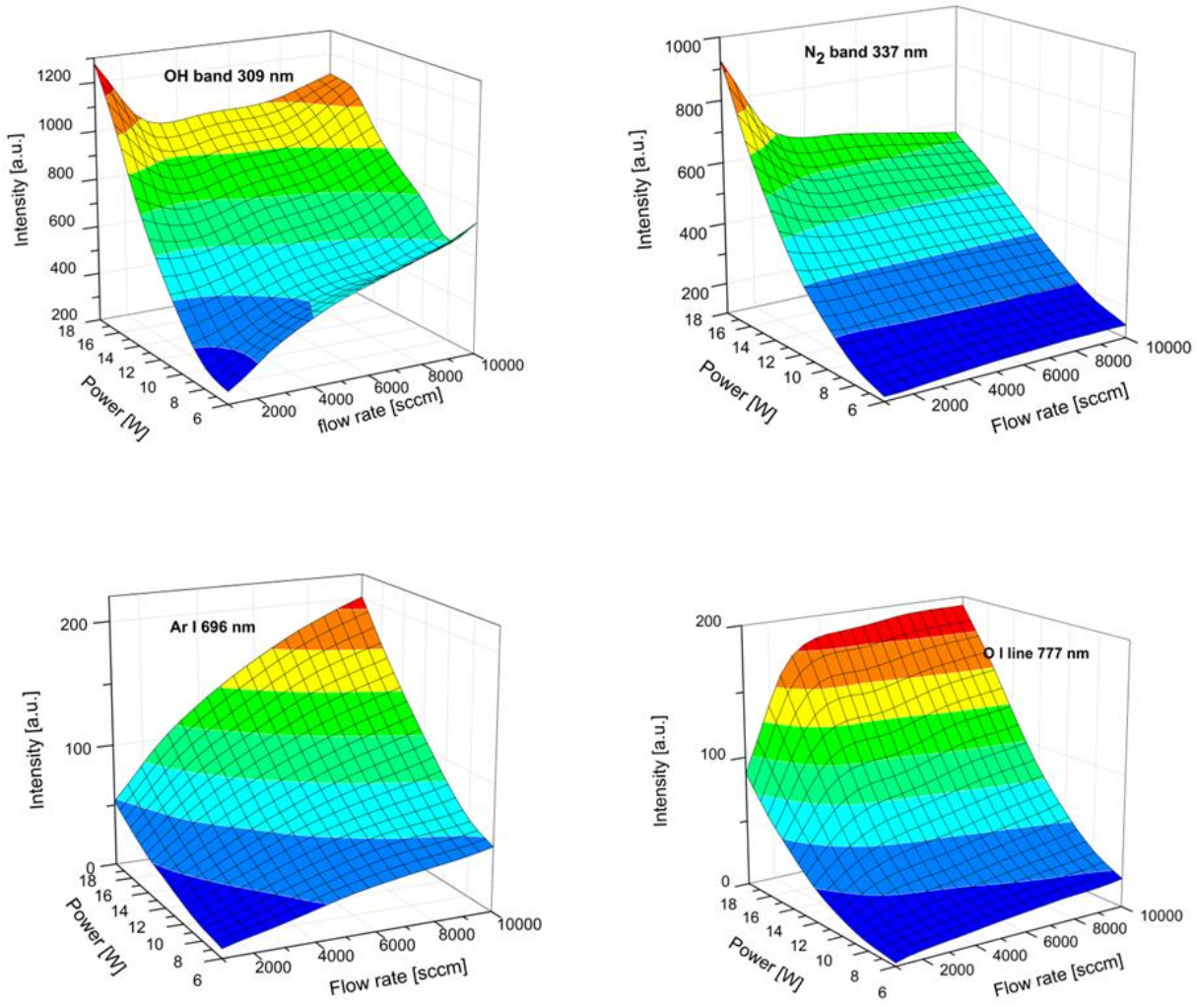

FIG. 5. Dependence of optical emission of OH (309 nm), N_2 (337 nm), Ar (696 nm) and O_2 (777 nm) on gas flow rate value and input power for **DBD** discharge configuration, in argon for RF power at the range of 6÷18 W (signal recorded at 1mm from nozzle, normal to the plasma plane.

The increasing of the intensities of all lines with increase RF power is observed for both sources. The increase clearly related to the fact that higher power results in longer afterglow. However, in DBD configuration the emission is almost linearly proportional to the power with the exception of 6 W where the discharge is probably not stable, see Figure 5. In DBE configuration emission tends to be saturated at power of around 18 W. We were not able to test higher power due to transfer of the discharge to γ filamentary mode. In both configurations (DBD and DBE) the intensities of OH and N_2 are highest at low mass flow rate value of 1 slm at power > 11 W. This is explained by strong mixing of the ambient air with the main Ar gas at such a low flow rate and so by increase of N_2 and H_2O amount in the afterglow. The increase of gas flow rate above the threshold of 1 slm at power >11 W leads

to formation of Ar laminar flow and increase of OH intensity as well as Ar I and O I. It indicates that the main source of H_2O in the discharge at flow rate higher than 1 slm is probably impurities in the gas and pipes and not the ambient air diffusion. The tendency in a change of the lines intensity is almost the same for both configurations of the source but all the intensities are 3÷5 times lower in DBD source which is also confirmed visually and by ICCD imaging.

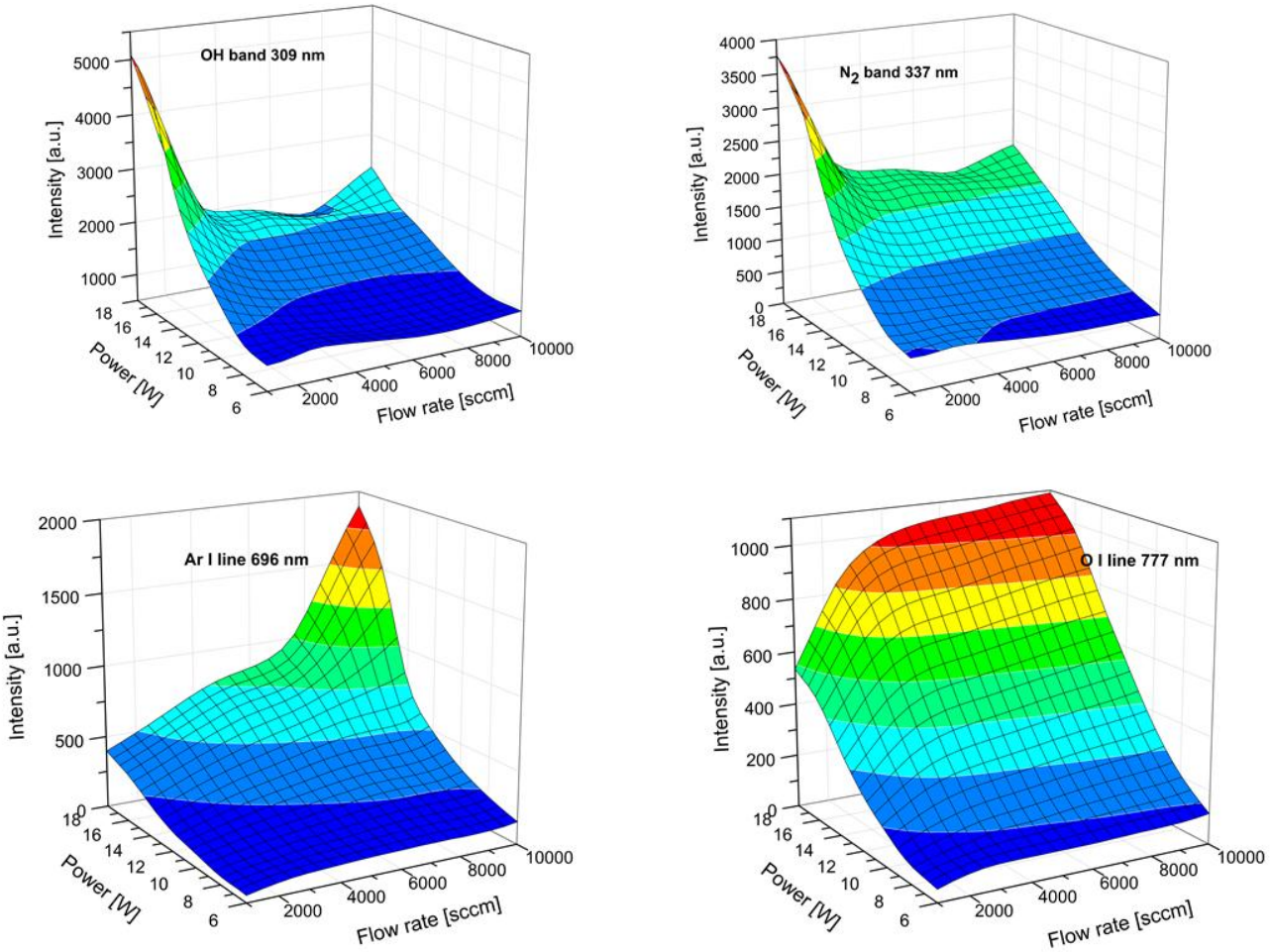

FIG. 6. Dependence of optical emission of OH (309 nm), N_2 (337 nm), Ar (696 nm) and O_2 (777 nm) on gas flow rate value and input power for **DBE** discharge configuration, in argon for RF power at the range of 6÷18 W (signal recorded at 1mm from nozzle, normal to the plasma plane.

Ar I signal is increasing with increase of the Ar flow rate in both discharges since increase of flow prevents plasma core from the air admixing. It has to be noted that intensity of O I line follows the behavior of Ar I in contrast to lines of OH and N_2^*. The particularity is observed for Ar I line in dependence of the used plasma source configuration. In barrier discharge Ar I signal increases gradually with increase of flow rate from 2 to 10 slm but in DBE source the Ar I emission has strong peak at power higher 16 W and flow of 8-10 slm. Such a difference in behavior of Ar I emission is probably related to transformation of α-mode to γ-mode characterized by much higher

intensity of Ar I lines. Strong dependence of the Ar I emission on the discharge mode can be useful tool to control operation of the source in applications in order to prevent transformation to γ-mode, e.g. through variation of the input power.

3.2. Imaging of the discharge.

In consideration of the possible application of the developed plasmas the length and structure of the afterglow are the key parameters. For the purpose of investigate the spatial distribution in the plasma jet, we used imaging of DBD and DBE plasma jets with band-pass filters (FWHM=10 nm) with maximum of transparency at 309 nm (maximum of OH (A) emission) and 753 nm (Ar I line), placed in the front of camera, and also images were made without filter. For pictures analysis a region of interest (ROI) has been defined from which the horizontal and vertical integral intensity profile were extracted, as shows in Figure 7.

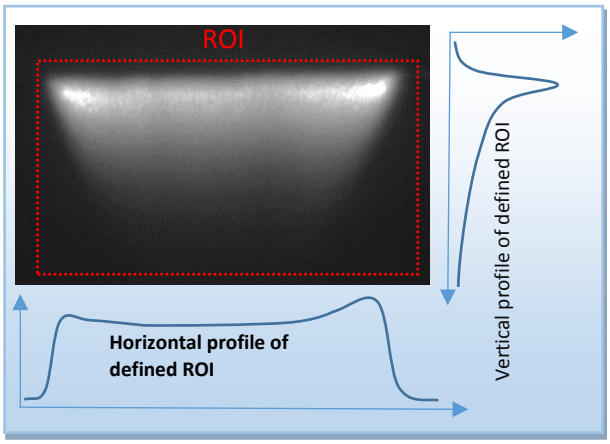

FIG. 7. Sample image of the DBD plasma jet, which shows how the horizontal and vertical intensity profiles were extracted, and a region of interest (ROI) determination.

The profile intensities were calibrated with camera gain factor in order to account the fact that the images were taken with different camera gain values. The calibration of the camera has been carried out with the same Oriel lamp as one used for the absolute calibration of the spectrometer. Figure 8 shows a comparison between the optical emission intensity profiles, along the plasma jet (vertical), for DBD and DBE discharge, in argon with gas flow rate of 10 slm and input power of 12 W. The total emission of the discharge is almost 50 times higher for DBE discharge than for DBD discharge, see Figure 8, 9. Based on our experiments we can see that presence of the dielectric barrier helps for ignition of the discharge and sustaining the plasma in diffuse mode but the total emission from the plasma volume is considerable lower as confirmed by ICCD images presented in figure 8,9. The stabilization effect of the barrier discharge is demonstrated in figure 9 for horizontal distribution of the light intensity in the discharge zone.

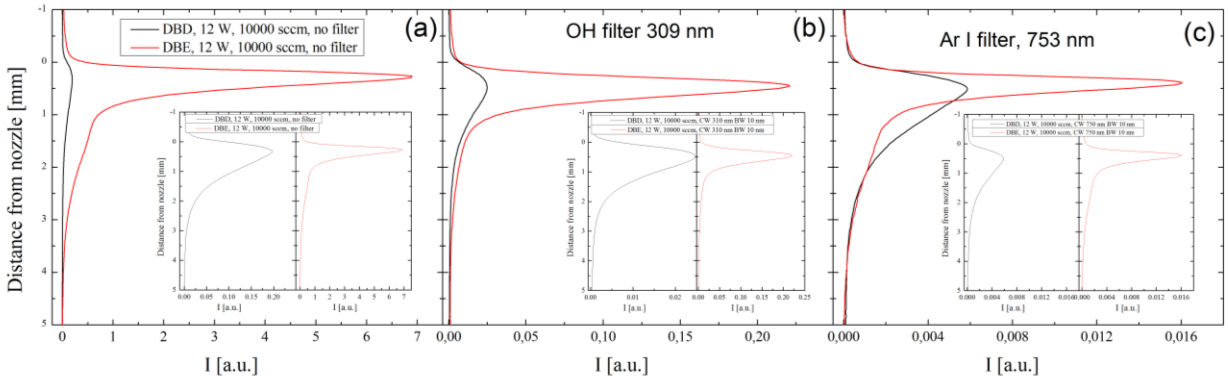

FIG. 8. Comparison between the optical emission intensity profiles, along the plasma jet (vertical), for DBD and DBE discharge, in argon at 10 slm and 12 W RF power; without filter (a), with CW 309 nm (b) and CW 753 nm with 10 nm BW.

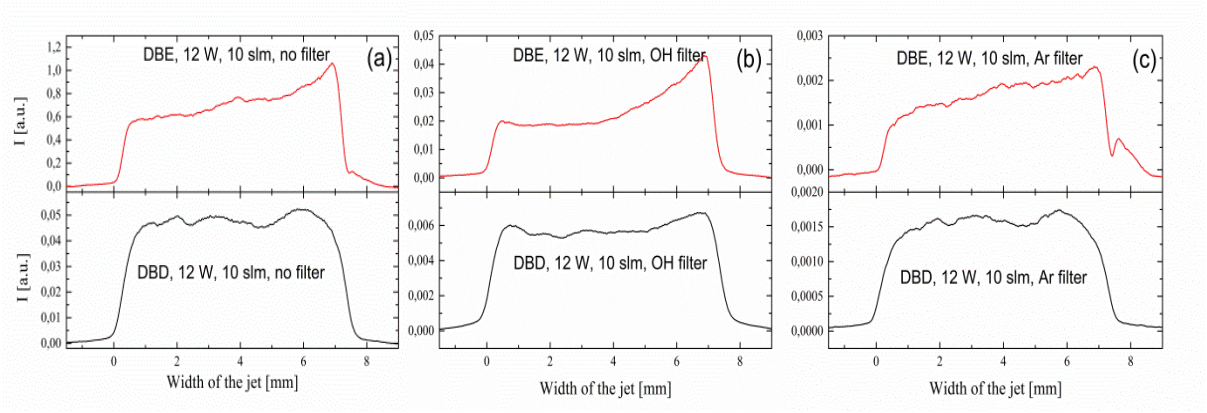

FIG. 9. Comparison between the optical emission intensity profiles, across the plasma jet (horizontal), for DBE (top) and DBD (bottom) discharge, in argon at 10 slm gas flow and 12 W RF power; without filter (a), with 309 nm filter (b) and 753 nm filter (c).

Though emission from DBE discharge is much higher than that from DBD, the profile is smother in the latter with very little of oscillations along the nozzle. In DBE configuration even small imperfections in the construction of the source and on surface of the metal electrodes lead to strong change in the local discharge intensity as we see in figure 9 (c) at 7 mm. The charge accumulation on dielectric barrier in DBD configuration allows to obtain uniform distribution of the electrical field in the gap and so to stabilize the plasma. The clear drawback of the presence of the barrier is related to its effect on direct current in RF plasmas. Purely capacitive coupling in DBD source leads to lower current by compare with the current in DBE configuration and so in formation of much weaker discharge.

3.3. Continuum Bremsstrahlung radiation analysis

As shown in section 3.2 presence of the dielectric barrier has strong influence on the source performance but the picture of the discharge analysis will be incomplete without study of its electron density and temperature. RF plasma source designed in the present work emits strong continuum Bremsstrahlung radiation, see Figure 4 interval 350-600 nm. This kind of continuum is well known phenomena in low pressure high ionized discharge and usually attributed to electron ions interactions. In high pressure low ionization degree plasma, as one considered here, the appearing of continuum is a result of 3 processes attributed to electron-atom, electron-ion free-free, and electron-ion free-bond interactions [23]. In present work, the absolute value of the plasma continuum emissivity in W × $nm^{-1}m^{-3}sr^{-1}$ due to the Bremsstrahlung radiation is calculated as a sum of the contribution from electron–atom interactions: $\varepsilon_{ea}(\lambda, T_e, n_e)$, from recombination of electrons and ions: $\varepsilon_{ei}^{fb}(\lambda, T_e, n_e)$, and from free-free interaction of electrons and ions: $\varepsilon_{ei}^{ff}(\lambda, T_e, n_e)$. In approximation of Maxwellian energy distribution of the electron energy the continuum contributions can be expressed as [23,24]:

$$\varepsilon_{ea}(\lambda, T_e, n_e) = C_{ea}\frac{n_e n_{Ar}}{\lambda^2 (k_b T_e)^{3/2}}\int_{hc/\lambda}^{\infty} Q_{ea}^{mom}(E)\left(1-\frac{hc}{2\lambda E}\right)\sqrt{1-\frac{hc}{\lambda E}}\times \exp(-E/k_b T_e)\times E^2 dE \quad (1)$$

$$\varepsilon_{ei}^{fb}(\lambda, T_e, n_e) = C_1 Z^2 \frac{n_e n_i}{\lambda^2\sqrt{T_e}}\left(1-exp\left(\frac{hc}{\lambda k_b Te}\right)\right)\xi_{ei}^{fb}(\lambda, T_e) \quad (2)$$

$$\varepsilon_{ei}^{ff}(\lambda, T_e, n_e) = C_1 Z^2 \frac{n_e n_i}{\lambda^2\sqrt{T_e}} exp\left(\frac{hc}{\lambda k_b Te}\right)\xi_{ei}^{ff}(\lambda, T_e) \quad (3)$$

where n_{Ar} is a density of Ar atoms, λ is a wavelength, E is a electrons energy, k_b is the Boltzmann constant, n_i is a density of the ions, Z is a charge of the ions and $Q_{ea}^{mom}(E)$ is the momentum transfer cross section for electron atoms collisions. The constants in eq.(1-3) are $C_{ea} = 0.10779 \times \frac{\alpha h}{m_e^{3/2} c}\ Wm^2 J^{-3/2} sr^{-1}$ with $\alpha = \frac{e^2}{2hc\varepsilon_0}$, ε_0 is the permittivity of vacuum, $C_1 = 1.6321 \times 10^{-43}\ Jm^4 K^{1/2} s^{-1} sr^{-1}$ and $\xi_{ei}^{fb}(\lambda, T_e)$ and $\xi_{ei}^{ff}(\lambda, T_e)$ are the Biberman factors. As follows from eq. (1-3) the emissivity of the continuum depends on electron density and electron temperature and, correspondingly, both plasma parameters can be estimated based on eq. (1-3) if absolute value of the plasma continuum is measured. As calculation of the integral in eq. (1) is very time consuming, a number of approximation equations have been proposed, see e.g. [25,26] where two equations for lowest and highest limit of eq. (1) were tested. In contrast to works [24,25] here all the contributions from ε_{ea}, ε_{ei}^{ff}, and ε_{ei}^{fb} were considered and the integral in eq.(1) $\int_{hc/\lambda}^{\infty} Q_{ea}^{mom}(E)\left(1-\frac{hc}{2\lambda E}\right)\sqrt{1-\frac{hc}{\lambda E}}\times \exp(-E/k_b T_e)\times E^2 dE$ has been calculated numerically in Python v.2.7. The required value of Q_{ea}^{mom} is taken from [23], and so called Biberman factor ξ_{ei}^{ff} is considered as a constant in the wavelength range of 300-700 nm, whereas ξ_{ei}^{fb} is taken from [26]. The contribution of electron atom and electron ions collisions for two typical conditions of atmospheric pressure Ar discharge with T_g=330 K in the wavelength range 300-650 nm are presented in figure 10. The wavelength region for the simulation

is chosen considering the sensitivity range of the available spectrometers and the fact that calibration of the lamp was valid only for wavelength above 300 nm.

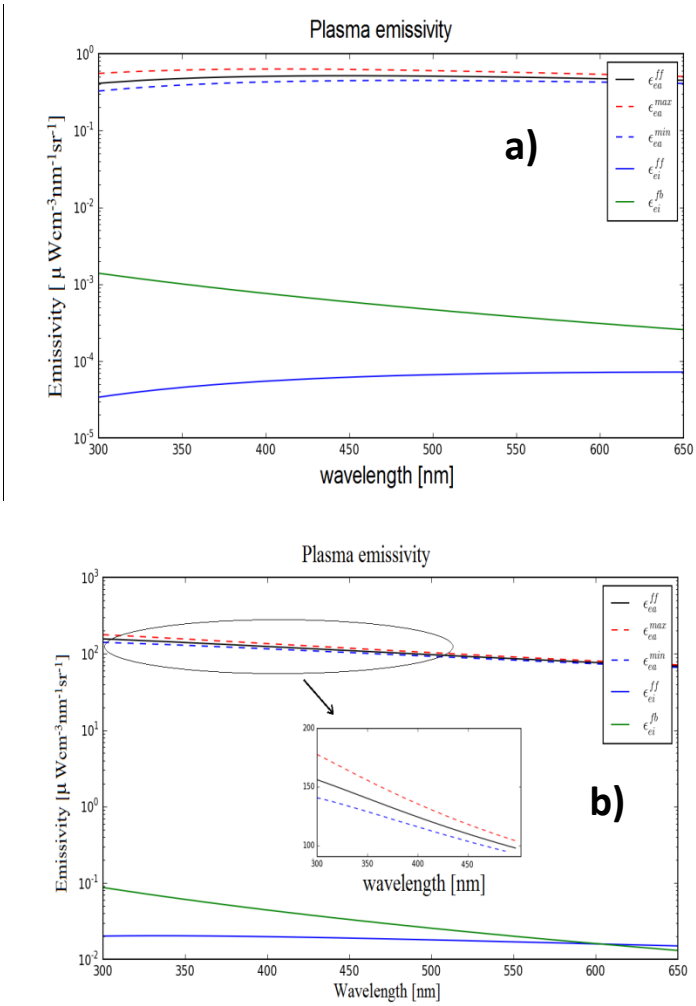

FIG. 10. Emissivity of the Ar plasma estimated through numerical solution of eq. 1-3 for two typical conditions: a) T_e=1 eV, n_e=10^{13} cm^{-3} and b) T_e=2 eV, n_e=10^{14} cm^{-3}. Values ε_{ea}^{max} and ε_{ea}^{min} are calculated through the use of approximation of the integral in eq.1 based on equations proposed in [23-25]. The emissivity is shown in log scale with inset in part b) demonstrating the approximations of eq.(1) in a linear scale.

The results of calculation show that at typical electron density realized in RF plasma jets of about 10^{13}-10^{14} cm^{-3} the contribution from the electron-ion interactions is 2-3 orders of magnitude lower than one from the electron-atom interactions ε_{ea}. The ε_{ei}^{ff}, and ε_{ei}^{fb} contributions start to be comparable with ε_{ea} at n_e >10^{16} cm^{-3} which is obviously cannot be reached in our experimental conditions. The continuum radiation level is higher in UV region and also as it will be shown below the UV part is more sensitive to the change of T_e and n_e. The obtained continuum emissivity presented in figure 10 has been compared with experimental results of absolute spectroscopy. It is important to note here that in our work the irradiance of the discharge in units W/nm × m^2 has been obtained instead

of the emissivity in $Wnm^{-1}m^{-3}sr^{-1}$ because of the used calibration procedure. The calculated in Figure 10 emissivity has been recalculated to the irradiance considering the emitting volume of the discharge measured with ICCD device and distance from the discharge to the detector. Furthermore, the irradiance of the plasma has been compared with results of the calculations based on eq. (1-3) and n_e with T_e have been determined. ε_{ea}, ε_{ei}^{ff}, and ε_{ei}^{fb} values have been calculated for the range of the electron densities of $10^{11} \div 10^{15}$ cm^{-3} and T_e varying from 0.5 to 2 eV. The value of the total irradiation considering all 3 contributions as a function of electron density is presented in Figure 11. Figure 12 shows an effect of the electron temperature on plasma continuum irradiation.

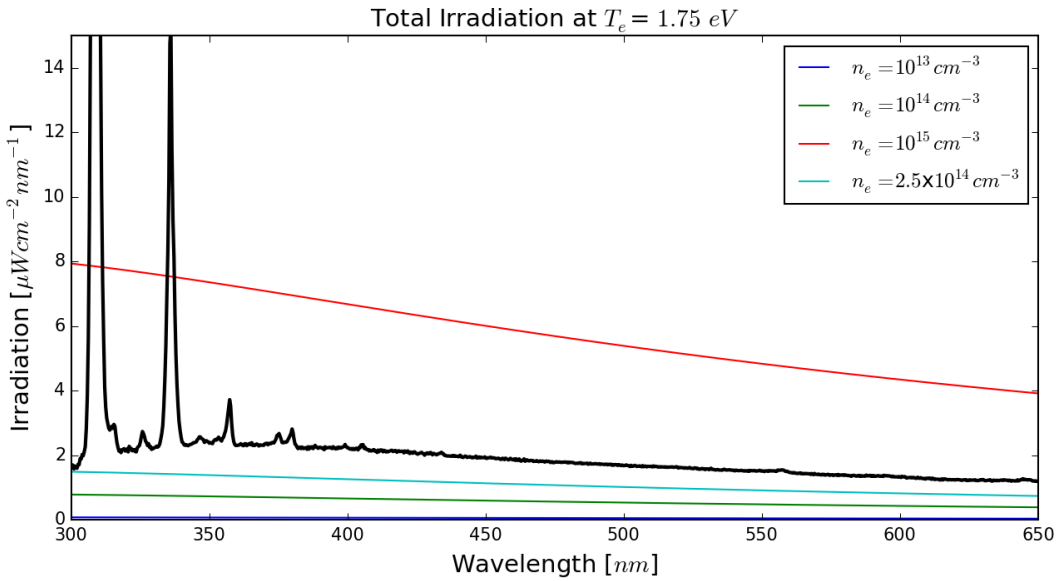

FIG. 11. Effect of electron density on the continuum radiation emitting by Ar discharge at atmospheric pressure for electron temperature of 1.75 eV. The black line represents a part of the absolutely calibrated experimental spectra of the discharge of 6 W input RF power working without the dielectric barrier: DBE configuration.

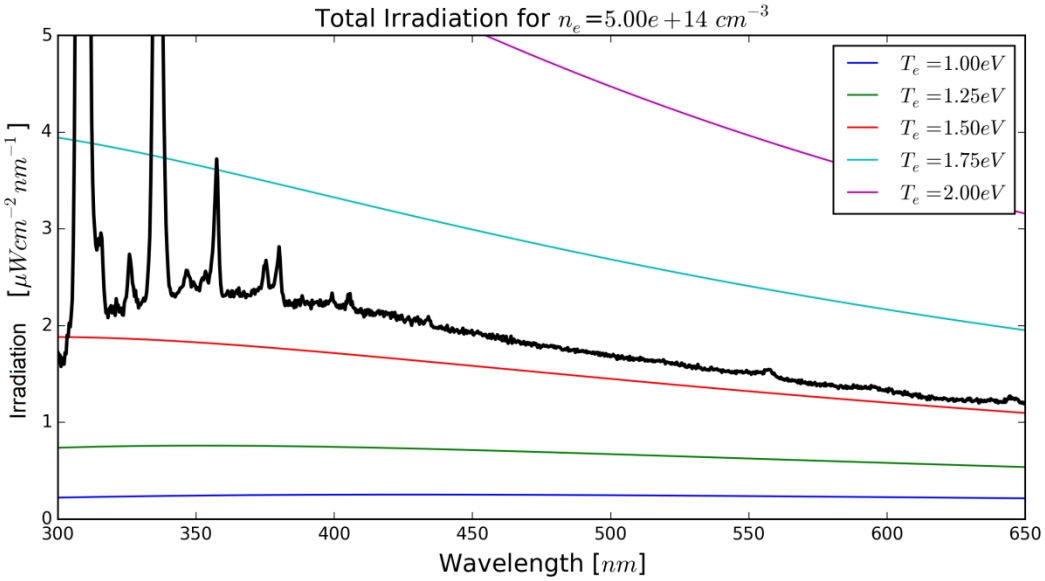

FIG. 12. Effect of electron temperature on the continuum radiation emitting by Ar discharge at atmospheric pressure for electron density of 5×10^{14} cm^{-3} and ion density equivalent to the electron density (DBE configuration).

The best fitting of the experimental results for RF plasma of 10 W, 5 slm working without the dielectric barrier (DBE) has been obtained with N_e=1.9±1×10^{20} m^{-3} and T_e=1.75±0.25 eV. The electron density measured through the absolute value of the continuum is in a good agreement with results obtained by different techniques [27] for RF atmospheric pressure plasma jets. The electron temperature is higher than the typical value of Ar excitation temperature T_{exc} of 1 eV measured in the plasma jets by line-ratio technique [28]. It has to be noted here that so called excitation temperature measured by means of the line-ratio method is actually not the electron temperature and special procedure has to be used to make a correction in estimation of T_e from T_{exc}. The value of T_e found here is in agreement with scarce direct measurements of T_e by Thomson scattering on plasma jet source of 14.5 MHz where T_e has been found of about 1.5 eV [29]. Based on experimental results in presented work it was revealed that variation of gas flow rate from 0.5 to 10 slm has very minor effect on n_e. A little bit higher n_e of 2.5±1×10^{20} m^{-3} has been determined for DBE plasma source at highest flow rate of 10 slm in comparing with n_e=1.5±1×10^{20} m^{-3} at 0.5 slm which is probably explained by air diffusion in to the discharge gap at gas flow rate of 0.5 slm. Correspondingly, the presence of O_2 in the discharge gap at very low flow rate leads to electron attachment $O_2 + e \rightarrow O_2^-$ and so to decrease of the electrons density. The increase of gas flow to maximum 10 slm had almost negligible effect on electron temperature for both configurations of the plasma source: with and without dielectric barrier. It was found that increase of the RF power from 6 to 18 W does not has any significant effect on electron density and electron temperature in both configurations of the plasma source: DBD and DBE. This is probably can be explained by our observation that power increase results in plasma expansion and formation of the longer afterglow. Correspondingly, the observed increase of the plasma irradiance is related to increase of the plasma emitting volume, as shown in the subchapter 3.2, whereas the plasma properties are kept constant. This observation

is beneficial in terms of possible upscale of the system as we can vary the input power of the up-scaled source without altering the plasma properties. Nevertheless, the use of dielectric barrier covering electrode has pronounced effect on the plasma operation. Use of the plasma source with dielectric barrier (DBD) results in formation of plasma with almost 6 times lower ionization degree by compare with DBE configuration. The measured electron density in DBD discharge of 10 W, 5 slm is about $0.38\pm0.3\times10^{20}$ m^{-3} which is much lower than $n_e = 1.9\pm1\times10^{20}$ m^{-3} measured for the same operational conditions in DBE plasma source. This fact is well agree with results of emission spectroscopy presented in Figure 5,6 for Ar lines intensities which are almost 10 times higher in DBE configuration. The effect of barrier layer on electrodes has shown less effect on electron temperature which is 1.75±0.25 eV and 1.5±0.25 eV in DBE and DBD configurations, respectively. Such a difference in T_e is within the errors of the method and no confirmed conclusions can be derived without independent measurements with higher sensitivity e.g. Thomson scattering which is out of the scope of the present study.

4. Conclusions

In summary, 8 mm wide diffuse RF planar discharge working at atmospheric pressure argon is developed and studied in current work. The main parameters of the discharge are determined in function of gas flow rate, input RF power and presence of dielectric barrier on the electrodes.

The gas temperature is estimated based on simulation of the rotational temperature of the OH radicals. In the considered here range of RF power variation (6-18 W), and flow rate (0.5-10 slm) variation the gas temperature of the afterglow is almost constant and is about 330±50 K.

The discharge emission is almost 10 times lower when dielectric barrier is used. However, ICCD imaging of the discharge afterglow indicates that in DBD configuration (with dielectric barrier) more stable and uniform afterglow up to 6 mm in a length can be formed whereas in DBE configuration 8 mm long afterglow is non-uniform and tends to transfer to γ mode at lower input power.

The continuum radiation recorded in the wavelength range of 300-700 nm is considered to originate from Bremsstrahlung radiation mainly due to interaction of neutrals and electrons. The measurement of absolute value of the continuum is proposed to be a powerful tool in diagnostics of the low temperature plasmas and allows us to estimate both electron density and temperature. Electrons density and temperature about $1.59\pm1\times10^{20}$ m^{-3} and 1.75±0.25 eV, respectively, are estimated from the absolute value of the continuum radiation for the discharge without dielectric materials at flow rate of 5 slm and 10 W input power. In DBD configuration $n_e=0.38\pm0.3\times10^{20}$ m^{-3} and $T_e=1.5\pm0.25$ eV are found for the same plasma operational conditions.

Studied here RF source is proposed as alternative to widely used plasma jets of mm size as it has a 8 mm wide afterglow with length up to 6 mm and can be easily up-scaled to any required industrial demands. The source has been tested in two configurations: with and without a dielectric barrier on the electrodes and it was shown that in

both configurations the afterglow can be used in bio-medical applications where strong non equilibrium plasma of low temperature is required.

6. Acknowledgements

The work was partially supported by the FWO fund, project 1.5.005.13N. Part of the work and short stay of Dr. Eusebiu-Rosini Ionita in Gent University has been supported through the COST action MP1101. The financial support of the Romanian Ministry of National Education, UEFISCDI-CNCS, in the frame of the contract: PN-II-RU-PD-2012-3-0583 is gratefully acknowledged.

7. References

1. M. Laroussi and T. Akan 2007 *Plasma Process. Polym.* 4 (9), 777.
2. X. Lu, Z. Jiang, Q. Xiong, Z. Tang and Y. Pan 2008 *Appl. Phys. Lett.* 92 (15), 151504.
3. Z. Cao, J. L. Walsh and M. G. Kong 2009 *Appl. Phys. Lett.* 94 (2), 021501.
4. Q. Y. Nie, Z. Cao, C. S. Ren, D. Z. Wang and M. G. Kong 2009 *New J. Phys.* 11 (11), 115015.
5. C. Qian, Z. Fang, J. Yang and M. Kang 2014 *IEEE Trans. Plasma Sci.* 42 (10), 2438.
6. C. Zhang, T. Shao, Y. Zhou, Z. Fang, P. Yan and W. Yang 2014 *Appl. Phys. Lett.* 105 (4), 044102.
7. M. Ghasemi, P. Olszewski, J. W. Bradley and J. L. Walsh 2013 *J. Phys. D: Appl. Phys* 46 (5), 052001.
8. X. Pei, Z. Wang, Q. Huang, S. Wu and X. Lu 2011 *IEEE Trans. Plasma Sci.* 39 (11), 2276.
9. Y. Duan, C. Huang and Q. S. Yu 2007 *Rev. Sci. Instrum.* 78 (1), 015104.
10. J. Tang, W. Cao, W. Zhao, Y. Wang and Y. Duan 2012 *Phys. Plasmas*. 19 (1), 013501.
11. J. Tang, S. Li, W. Zhao, Y. Wang and Y. Duan 2012 *Appl. Phys. Lett.* 100 (25), 253505.
12. X. Li, J. Tang, X. Zhan, X. Yuan, Z. Zhao, Y. Yan and Y. Duan 2013 *Appl. Phys. Lett*. 103 (3), 033519.
13. W. Jiang, J. Tang, Y. Wang, W. Zhao and Y. Duan 2014 *Appl. Phys. Lett.* 104 (1), 013505.
14. X. Lu, S. Wu, P. K. Chu, D. Liu and Y. Pan 2011 *Plasma Sources Sci. Technol*. 20 (6), 065009.
15. J. Shi and M. G. Kong 2007 *Appl. Phys. Lett.* 90 (11), 111502.
16. B. Li, Q. Chen and Z. Liu 2010 *Appl. Phys. Lett.* 96 (4), 041502.
17. C. Tendero, Ch. Tixier, P. Tristant, J. Desmaison, P. Leprince 2006 *Spectrochimica Acta Part B* 61, 2 – 30.
18. U. Kogelschatz 2003 *Plasma Chemistry and Plasma Processing* 23, 1.
19. G. Dinescu, E.R. Ionita 2008 *Pure and Applied Chemistry* 80, 1919-1930.
20. M. Teodorescu, M. Bazavan, E. R. Ionita, G. Dinescu 2012 *Plasma Sources Sci. Technol.* 21, 055010.
22. Q. Xiong, A. Y. Nikiforov, M. Á. González, C. Leys and X. P. Lu 2013 *Plasma Sources Sci. Technol.* 22 (1), 015011.
23. E. Iordanova, N. De Vries, M. Guillemier and J. van der Mullen 2008 *J. Phys. D: Appl. Phys* 41 (1), 015208.
24. E. Restrepo and A. Devia 2004 *J. Vac. Sci. Technol.* A 22 (2), 377.

25. E. Iordanova, J. Palomares, A. Gamero, A. Sola and J. van der Mullen 2009 *J. Phys. D: Appl. Phys* 42 (15), 155208.

26. B. Broks, J. Keizer, R. Zijlmans and J. van der Mullen 2006 *Plasma Sources Sci. Technol.* 15 (4), 865.

27. A. Y. Nikiforov, C. Leys, M. A. Gonzalez and J. L. Walsh 2015 *Plasma Sources Sci. Technol.* 24 (3), 034001.

28. U. Fantz 2006 Plasma Sources Sci. Technol. 15 (4), S137.

29. B. van Gessel, R. Brandenburg and P. Bruggeman 2013 *Appl. Phys. Lett.* 103 (6), 064103.